Fragmentation and splitting of Gamow-Teller resonances in Sn(^{3}He,t)Sb charge-exchange reactions, A = 112–124

K. Pham, J. Jänecke, and D. A. Roberts
Department of Physics, University of Michigan, Ann Arbor, Michigan 48109-1120

M. N. Harakeh
Kernfysisch Versneller Instituut, Zernikelaan 25, 9747 AA Groningen, The Netherlands

G. P. A. Berg, S. Chang, J. Liu, and E. J. Stephenson
Indiana University Cyclotron Facility, Bloomington, Indiana 47405

B. F. Davis
University of Notre Dame, Notre Dame, Indiana 46556

H. Akimune and M. Fujiwara
Research Center for Nuclear Physics, Osaka University, Osaka 567, Japan
(Received 30 September 1994)

Fragmentation and splitting of the Gamow-Teller (GT) strength has been observed in a systematic study of the (^{3}He,t) charge-exchange reaction at $E(^3\text{He})$=200 MeV over the entire range of stable Sn isotopes. Triton energy spectra were observed with a high-resolution magnetic spectrometer at angles near $\theta = 0°$ where $\Delta L = 0$ transitions are enhanced. Excitation energies, widths, 0° cross sections, and strengths B(GT) were determined. A theoretically predicted configuration splitting of the main Gamow-Teller component into two components, expected to be dominant near A =118 at the onset of the filling of the $1h_{11/2}$ neutron orbital, could not be observed. This may be due to the fact that the total widths of the resonances of 5–6 MeV exceed the predicted splitting. A comparison of the 0° cross sections for the transitions to the Gamow-Teller resonances and the isobaric analog states leads to strengths B(GT) for the main Gamow-Teller components of typically 65% of the sum-rule value of $3(N - Z)$. Three to four additional Gamow-Teller fragments ("pygmy resonances") were observed in all final nuclei at lower excitation energies. The excellent energy resolution of the experiment made it possible to observe a pronounced fine structure in these low-lying resonances which is believed to be due to coupling to two-particle–two-hole doorway states. Also seen with all target nuclei was a systematic sequence of strong J^π=1^+ states near the ground states in all Sb isotopes (E_x = 0 to 220 keV). In addition, strong $\Delta L = 1$ resonances were observed in all nuclei at excitation energies of typically 20 MeV. Furthermore, nonresonant background from quasifree charge exchange was observed. An average of ~85% of all excess neutrons seems to contribute to this background in approximate agreement with results from $(e, e'p)$ experiments.

PACS number(s): 24.30.Cz, 25.55.Kr, 27.60.+j

I. INTRODUCTION

Experimental Gamow-Teller (GT) strength below the isobaric analog states (IAS) was initially observed in light nuclei (e.g., Refs. [1–4]). However, charge-exchange reactions play a most important role in the study of Gamow-Teller resonances at higher excitation energies. Early investigations with the (p, n) reaction in the 25–45 MeV range [5–8] were followed in the early 1980's by systematic studies at energies >100 MeV [9–12]. Collective spin-flip resonances, including Gamow-Teller resonances, are preferentially excited at higher bombarding energies. The approximate proportionality between the Gamow-Teller strength B(GT) and 0° cross sections in this energy domain contributed significantly to the understanding of Gamow-Teller strength in nuclei [12,13]. (^{3}He,t) charge-exchange reactions, used extensively in the study of isobaric analog states at bombarding energies ≤30 MeV (e.g., Refs. [14,15], and references therein), are increasingly employed in the investigation of Gamow-Teller resonances [16–19]. It appears that despite certain differences in the reaction mechanisms for (p, n) and (^{3}He,t) charge exchange, there exists a close correspondence between the characteristics of the two reactions at the same energy per nucleon (e.g., Ref. [17]). Furthermore, the study of (^{3}He,t) reactions with magnetic spectrometers, including the study at $\theta = 0°$, has the advantage of superior energy resolution combined with high ejectile detection efficiency and large solid angle. As a result the investigation of subsequent proton and neutron decays and hence the study of the microscopic structure of giant resonances has become possible (e.g., Refs. [18,19]).

Theoretical discussions concerning the possible existence of collective J^π=1^+ states with structures related to isobaric analog states have been reported by Ikeda, Fujii, and Fujita [20] many years prior to their experimental observation. Another important prediction was

obtained in a quasiclassical treatment [21,22] where the authors point out that the high-lying 1^+ states with maximum collectivity are related to isobaric analog states, and that the Wigner supermultiplet scheme [23] provides a description of their common spin-isospin characteristics.

In addition to the main Gamow-Teller components at excitation energies slightly above the isobaric analog states and associated with the excitation of neutrons into proton orbits (spin-orbit partners), $j = \ell + \frac{1}{2} \rightarrow j = \ell - \frac{1}{2}$, the authors also predicted the existence of low-lying Gamow-Teller fragments associated with $j \rightarrow j$ "core-polarization" and $j = \ell - \frac{1}{2} \rightarrow j = \ell + \frac{1}{2}$ "back-spin-flip" transitions. Whereas there exist only two weak Gamow-Teller fragments within the framework of this simplified shell-model treatment (three-level model) [21,22,24], fragmentation into three and more low-lying slightly collective states of the particle-hole type [25,26,24,16,27,28] is expected and is determined by the number of discrete and quasidiscrete Gamow-Teller particle-hole configurations.

A configuration splitting of the main Gamow-Teller component has also been predicted recently by Guba, Nikolaev, and Urin [24] for the Ge and Sn isotopes. For the Sn isotopes the splitting is caused by the small energy difference between the $(1h_{9/2})(1h_{11/2})^{-1}$ particle-hole configuration and the main component containing all other configurations carrying the Gamow-Teller quantum numbers. This energy difference is the result of neutron pairing which becomes important when the $1h_{11/2}$ neutron level is close to the Fermi energy.

Fragmentation of the Gamow-Teller strength into three or more components has been observed recently [16] in the (^{3}He,t) charge-exchange reaction on targets of ^{117}Sn and ^{120}Sn. However, the predicted configuration splitting of the main Gamow-Teller component near $A \approx 118$ could not be observed possibly because the total widths Γ exceed the predicted splitting. It was the purpose of the present investigation to study the various effects systematically with the (^{3}He,t) charge-exchange reaction at $E(^3\text{He}) = 200$ MeV near $\theta = 0°$ with good energy resolution over the entire range of stable Sn isotopes from $A = 112$ to 124. Preliminary results have been reported previously [29,30].

Experimental techniques, the data reduction, and experimental results are presented in Secs. II and III. This is followed in Sec. IV by a detailed discussion of the observed phenomena.

II. EXPERIMENTAL TECHNIQUES AND DATA REDUCTION

The experiment was carried out at the Indiana University Cyclotron Facility (IUCF) with a beam of 200 MeV ^{3}He particles and currents of ~25 nA (electrical). Tritons from the (^{3}He,t) reaction were detected in the focal plane of the K600 high-resolution magnetic spectrometer [31,32]. Details of the experimental techniques used to measure spectra near $\theta = 0°$ have been described before [15,16] and will only be reviewed briefly here.

Reaction products as well as the incident $^3\text{He}^{2+}$ beam enter the magnetic spectrometer. The beam with its lower magnetic rigidity (factor of ~2) is bent inward towards an electrically insulated beam stop. Tritons are detected in the focal-plane detection system consisting of two multiwire drift chambers backed by two scintillation detectors for particle identification and drift-time measurements. The ray-tracing capabilities allow the simultaneous measurement of triton spectra at $\theta \approx 0°$ and $\theta \approx 2°$ using a rectangular aperture centered at $\theta = 1°$ and position information from both drift chambers. This provides an important signature for the identification of $\Delta L = 0$ transitions which were found to decrease sharply in cross section for angles $\theta > 0°$. Since transitions to states and resonances with $\Delta L > 0$ as well as nonresonant background have cross sections which change much more slowly with angle, the difference spectra for the two angles become very sensitive to $\Delta L = 0$ contributions. Spectra measured at $\theta \approx 0°$, $\theta \approx 2°$, and the difference spectra are shown in the next section. They confirm this expectation.

The effective length of the focal-plane detector covered an energy range of $\Delta E/E \approx 16$ % and hence a region of excitation energies of ~30 MeV. Some instrumental background at low magnetic rigidity (high E_x) was produced by the beam stop but could be identified and removed by

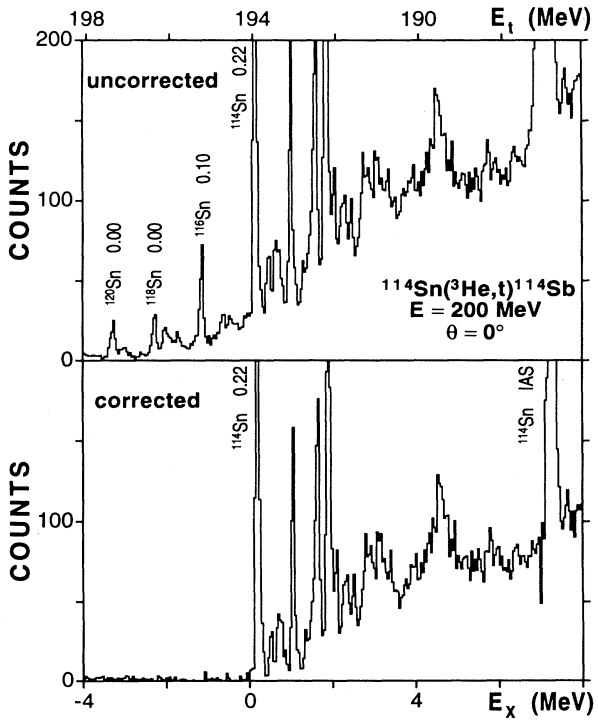

FIG. 1. Triton energy spectra for ^{114}Sn(^{3}He,t)^{114}Sb at $E(^3\text{He}) = 200$ MeV and $\theta \approx 0°$ for the region of low excitation energies (top). The second spectrum (bottom) has been corrected for the presence of ^{116,118,120}Sn in the target (~30%). The measured momentum spectra are linearized in energy.

TABLE I. Thicknesses and isotopic abundances for the targets used in the present experiment.

Target	Enrichment (%)	$\rho\Delta x$ (mg/cm^2)
^{112}Sn	98.9	2.6
^{114}Sn	71.1[a]	2.7
^{116}Sn	95.6	2.2
^{117}Sn	89.2	2.4
^{118}Sn	97.8	2.5
^{119}Sn	89.8	2.6
^{120}Sn	98.4	2.2
^{122}Sn	95.4	2.5
^{124}Sn	97.2	2.7

[a] ^{116}Sn, 10.2 %; ^{118}Sn, 6.3 %; ^{120}Sn, 5.9 %.

using spectra from an empty target frame. The particle identification in the focal plane with the two plastic scintillators was very good, and the energy resolution, mostly due to target thickness, was ~80 keV.

All targets used in the experiment were isotopically enriched self-supporting Sn targets. The isotopic enrichments and the target thicknesses of typically 2.5 mg/cm^2 are listed in Table I. Only the ^{114}Sn target had a low isotopic abundance of only ~70%. The presence of ^{116,118,120}Sn in this target is obvious from the uncorrected 0° spectrum for low E_x shown in Fig. 1. However, also shown in the figure is a clean corrected spectrum obtained by subtracting properly normalized measured spectra for these components.

Both on-line and off-line data acquisition was carried out with the powerful multiparameter program XSYS [33]. The measured position spectra (momentum spectra) are slightly nonlinear in energy. All figures shown in this work display spectra which were linearized in energy allowing for a more convenient comparison of the spectra obtained with different targets.

The energy calibration made use of known discrete calibration lines including the isobaric analog states [34], low-lying states [35], and the peaks seen at 200 MeV from singly ionized ^{3}He$^+$ ions [36]. The global energy calibration was carried out for all spectra simultaneously, and the energy uncertainty for the sharp states is estimated as ±30 keV.

III. EXPERIMENTAL RESULTS

Figure 2 shows triton energy spectra for the reaction ^{118}Sn(^{3}He,t)^{118}Sb up to excitation energies of ~28 MeV with an energy binning of 120 keV/channel. The spectra (a) and (b) were obtained for angles of $\theta \approx 0°$ and $\theta \approx 2°$, respectively, and spectrum (c) represents the difference. The spectra display broad structures and sharp states including the known J^π=1$^+$ ground state and J^π=0$^+$ isobaric analog state at E_x = 9.33 MeV. As expected, the difference spectrum (c) enhances the ΔL =0 transitions including the broad main Gamow-Teller resonance at E_x = 10.6 MeV (labeled GT1), several lower-lying components (labeled GT2 and GT3), the J^π=1$^+$ ground state, and the J^π=0$^+$ isobaric analog state. A higher-lying resonance [labeled ΔL = 1 in spectrum (b)] and nonresonant background cancel to a large extent. Solid lines are included in the spectra. They were obtained from a fitting procedure described in Sec. IV A.

Figure 3 shows the same spectra as Fig. 2, again for angles of $\theta \approx 0°$, $\theta \approx 2°$, and the difference spectrum, but here only for excitation energies up to E_x = 8 MeV and with an energy binning of 40 keV/channel. Interestingly, very pronounced fine structures of the low-lying resonances GT2, GT3, and GT4 become apparent. Most

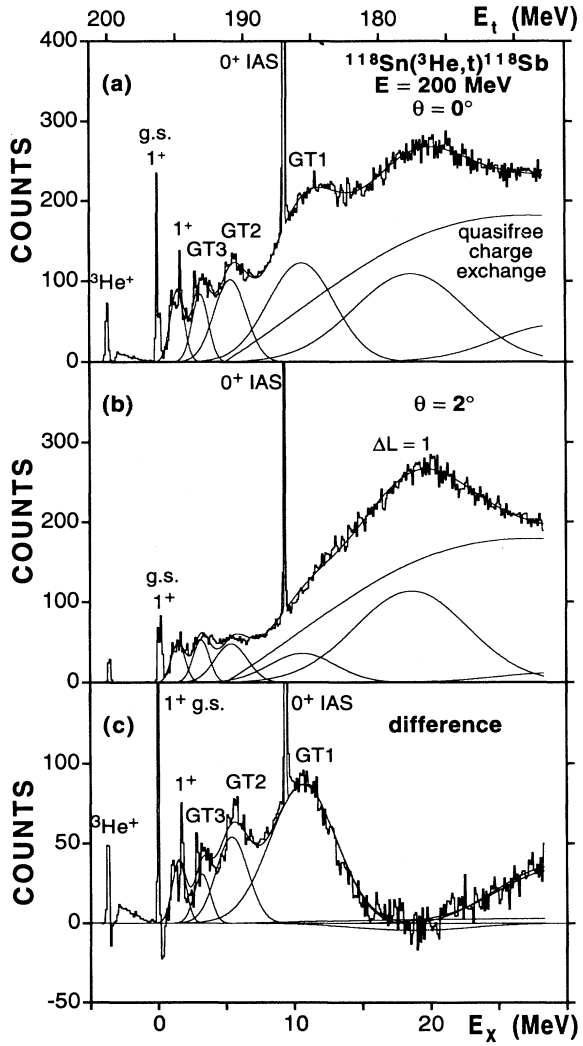

FIG. 2. Triton energy spectra for ^{118}Sn(^{3}He,t)^{118}Sb at E(^{3}He) = 200 MeV and (a) $\theta \approx 0°$ and (b) $\theta \approx 2°$. Spectrum (c) displays the difference between the spectra (a) and (b). The measured momentum spectra are linearized in energy and cover excitation energies up to $E_x \approx$ 28 MeV with a binning of 120 keV/channel. The solid lines are obtained from a fitting procedure as discussed in the text.

TABLE II. Experimental excitation energies, widths, and cross sections at $\theta = 0°$ from ^{A}Sn(^{3}He,t)^{A}Sb, A = 112–124, at $E(^{3}\mathrm{He}) = 200$ MeV.

A	IAS E_x (MeV)	IAS $d\sigma/d\Omega$ (mb/sr)	GT1 E_x (MeV)	GT1 Γ (MeV)	GT1 $d\sigma/d\Omega$ (mb/sr)
112	6.16±0.03	5.4±0.3	8.94±0.25	4.8±0.3	12.4±1.5
114	7.28±0.03	5.1±0.3	9.39±0.25	5.6±0.3	14.3±1.7
116	8.36±0.03	6.0±0.4	10.04±0.25	5.5±0.3	16.8±2.0
117	11.27±0.03	5.9±0.4	12.87±0.25	5.8±0.3	17.6±1.0
118	9.33±0.03	6.2±0.4	10.61±0.25	5.7±0.3	17.2±2.1
119	12.36±0.03	6.7±0.4	13.71±0.25	5.7±0.3	19.6±2.4
120	10.24±0.03	7.1±0.4	11.45±0.25	6.4±0.3	24.2±2.9
122	11.24±0.03	8.1±0.5	12.25±0.25	5.6±0.3	21.9±2.6
124	12.19±0.03	7.3±0.4	13.25±0.25	5.2±0.3	21.5±2.6

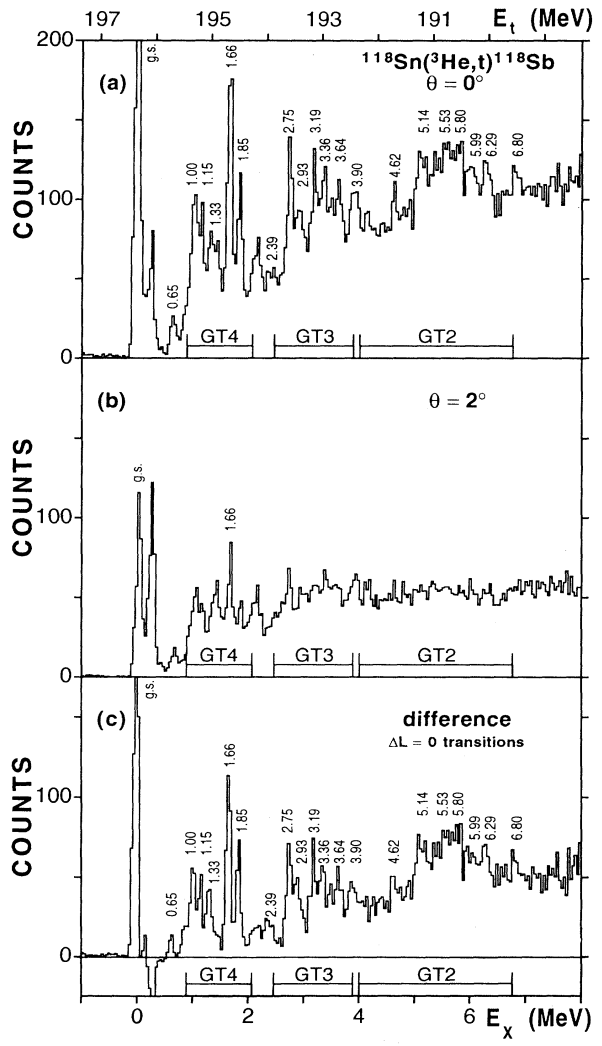

FIG. 3. Region of low excitation energies for the triton energy spectra of the reaction ^{118}Sn(^{3}He,t)^{118}Sb as shown in Fig. 2. The binning of the spectra by 40 keV/channel permits the observation of fine structures. The measured momentum spectra are linearized in energy.

TABLE III. Experimental excitation energies, widths, and cross sections at $\theta = 0°$ from ^{A}Sn(^{3}He,t)^{A}Sb, A = 112–124, at $E(^{3}\mathrm{He}) = 200$ MeV.

A	GT2 E_x (MeV)	GT2 Γ (MeV)	GT2 $d\sigma/d\Omega$ (mb/sr)	GT3 E_x (MeV)	GT3 Γ (MeV)	GT3 $d\sigma/d\Omega$ (mb/sr)
112	4.08±0.25	2.0±0.3	4.9±0 6	2.49±0.20	0.9±0.3	1.5±0.2
114	4.55±0.25	2.1±0.3	4.4±0.5	2.95±0.20	0.9±0.3	1.5±0.2
116	5.04±0.25	2.5±0.3	6.2±0.7	3.18±0.20	0.8±0.3	2.1±0.3
117	7.64±0.25	2.2±0.3	4.3±0.5	5.45±0.20	1.8±0.3	3.6±0.4
118	5.38±0.25	2.8±0.3	6.9±0.8	3.17±0.20	1.4±0.3	2.9±0.3
119	8.09±0.25	2.9±0.3	6.0±0.7	5.49±0.20	2.1±0.3	4.1±0.5
120	5.82±0.25	3.1±0.3	7.7±0.9	3.18±0.20	2.2±0.3	4.7±0.6
122	6.65±0.25	3.7±0.3	9.2±1.1	3.37±0.20	3.1±0.3	6.3±0.8
124	7.13±0.25	4.6±0.3	11.4±1.4	3.44±0.20	2.9±0.3	4.7±0.6

TABLE IV. Experimental excitation energies, widths, and cross sections at $\theta = 0°$ from ^{A}Sn(^{3}He,t)^{A}Sb, A = 112–124, at $E(^{3}\mathrm{He}) = 200$ MeV.

A	GT4 E_x (MeV)	GT4 Γ (MeV)	GT4 $d\sigma/d\Omega$ (mb/sr)	GT5 E_x (MeV)	GT5 Γ (MeV)	GT5 $d\sigma/d\Omega$ (mb/sr)
112	1.33±0.20	1.0±0.3	2.0±0.2			
114	1.88±0.20	0.6±0.3	1.8±0.2	0.90±0.20	0.7±0.3	0.7±0.1
116	1.84±0.20	1.1±0.3	2.5±0.3	0.74±0.20	0.5±0.3	0.7±0.1
117	3.87±0.20	1.0±0.3	1.5±0.2	2.98±0.20	0.5±0.3	0.6±0.1
118	1.47±0.20	1.2±0.3	2.6±0.3			
119	3.63±0.20	1.2±0.3	1.9±0.2			
120	1.38±0.20	0.6±0.3	1.8±0.2			
122	1.45±0.20	0.7±0.3	1.2±0.1			
124	1.50±0.20	0.9±0.3	1.6±0.2			

TABLE V. Doorway states with $\Delta L = 0$ in Sb nuclei with excitation energies and cross sections at $\theta = 0°$ (see text). w = weak; $d\sigma/d\Omega < 400$ μb/cm^2; energy uncertainties ±30 keV.

A	E_x (keV)	$d\sigma/d\Omega$ (μb/sr)	A	E_x (keV)	$d\sigma/d\Omega$ (μb/sr)	A	E_x (keV)	$d\sigma/d\Omega$ (μb/sr)
112	140	914	114	220	1013	116	100 [a]	951
	510	w		540	w		760 [a]	w
	850	431		1070	349		930 [a]	w
	1120	w		1660	568		1160 [a]	w
	1340	608		1930	860		1370 [a]	w
	1540	w		2110	w		1680	w
	1830	725		2340	w		1830	w
	2180	w		2540	w		1980	w
	2410	w		2790	w		2280	614
	2720	531		2950	w		2520	w
	3100	w		3140	w		2780	w
	3420	w		3420	w		3080	w
	3680	w		3970	w		3350	666
	3850	461		4580	487		4520	w
	4050	w		4940	w		4770	w
	4240	w		5800	w		5010	w
	4600	w		6430	w		5260	w
	4880	w					5770	w
	5310	w						
	5570	w						

[a]State has been previously observed. See Table VIII.

TABLE VI. Doorway states with ΔL =0 in Sb nuclei with excitation energies and cross sections at $\theta = 0°$ (see text). w = weak; $d\sigma/d\Omega < 400$ μb/cm^2; energy uncertainties ±30 keV.

A	E_x (keV)	$d\sigma/d\Omega$ (μb/sr)	A	E_x (keV)	$d\sigma/d\Omega$ (μb/sr)	A	E_x (keV)	$d\sigma/d\Omega$ (μb/sr)
117	1720[a]	w	118	0[a]	843	119	1730[a]	w
	2280[a]	440		650	w		2320	465
	2880	w		1000	w		3280	w
	3140	w		1150	w		3440	w
	3490	w		1330	w		3620	w
	3820	w		1660	542		3990	w
	4160	w		1850	w		4200	w
	5080	w		2390	w		4490	w
	5550	w		2750	524		6880	w
	5850	w		2930	w		7200	w
	7520	w		3190	w			
				3360	w			
				3640	w			
				3900	w			
				4620	w			
				5140	w			
				5530	w			
				5800	w			
				5990	w			
				6290	w			
				6800	w			

[a]State has been previously observed. See Table VIII.

of these states display ΔL=0 characteristics. All identified $\Delta L = 0$ transitions are labeled by their excitation energies. Only one state close to the ground state is cleary identified with $\Delta L \neq 0$. No such fine structure is present for the main Gamow-Teller resonance.

The spectra of Figs. 2 and 3 for $A = 118$ were selected

TABLE VII. Doorway states with ΔL =0 in Sb nuclei with excitation energies and cross sections at $\theta = 0°$ (see text). w = weak; $d\sigma/d\Omega < 400$ μb/cm^2; energy uncertainties ±30 keV.

A	E_x (keV)	$d\sigma/d\Omega$ (μb/sr)	A	E_x (keV)	$d\sigma/d\Omega$ (μb/sr)	A	E_x (keV)	$d\sigma/d\Omega$ (μb/sr)
120	−10 [a]	979	122	70	704	124	150	723
	990	w		630	w		770	w
	1260	651		1350	1059		1330	478
	1530	636		1780	482		1500	423
	2110	w		2050	w		1870	w
	2630	w		2500	w		2050	w
	2930	w		2840	w		2410	w
	3260	w		3190	w		2850	w
	3480	w		3510	w		3090	w
	3790	w		4000	w		3280	w
	4080	w		4420	w		3600	w
	5040	w					3970	w
	5360	w					4150	w
	5540	w						
	6030	w						
	6290	w						
	6470	w						
	6800	w						

[a]State has been previously observed. See Table VIII.

TABLE VIII. Known states from Ref. [35] in Sb nuclei which correspond to identified doorway states (see Tables V–VII).

A	E_x (keV)	J^π
116	94	1^+
	732	1^+
	918	1^+
	1158	1^+
	1386	1, 2, 3
117	1716	$1/2^+$,$3/2^+$
	2285	$1/2^+$
118	0	1^+
119	1750	$(3/2^+)$
120	0	1^+

as examples, and the corresponding spectra obtained for all other targets display similar characteristics.

All spectra measured at $\theta = 0°$ show also a strong peak from singly ionized $^3He^+$ ions at 200 MeV produced by atomic charge exchange in the targets [36].

The parameters of the isobaric analog states and Gamow-Teller resonances including their low-lying components, i.e., the excitation energies E_x, total widths Γ, and cross sections $d\sigma/d\Omega(0°)$, are listed in Tables II, III, and IV for all target nuclei. The uncertainties of the excitation energies E_x and widths Γ are estimated to range from ±200 to ±300 keV. The excitation energies E_x and cross sections $d\sigma/d\Omega(0°)$ for all observed low-lying discrete states are listed in Tables V–VII. The energy uncertainties of these sharp states including the isobaric analog states are estimated, as already mentioned, at ±30 keV. The cross sections of the sharp lines do not include the underlying contributions from nonresonant background and the main Gamow-Teller resonance which were subtracted prior to the determination of the yields. Excitation energies for several lines included in Tables V–VII have been reported previously [35]. These states together with their spin-parity assignments J^π are listed in Table VIII.

IV. DISCUSSION

A. General considerations

The decomposition of the measured spectra into resonances and nonresonant components, as shown in Fig. 2 by the solid lines, makes use of a fitting procedure invoking analytical expressions. The nonresonant background, as outlined below in Sec. IV G, is described by a Lorentzian line shape multiplied by a cutoff term representing Pauli blocking [37,38]. Only two free adjustable parameters were used, and the remaining parameters were fixed at accepted values. The resonances are described by Gaussian line shapes with three free parameters each, the centroid energies, the widths, and the heights. The fitting procedure for the 0° and 2° data

employed an iterative technique since it was not possible to search for all parameters simultaneously. It must be noted, though, that the results are influenced by assumptions which include whether the presence of additional resonances is assumed or not. Candidates for such resonances are the $T = T_0$ component of the Gamow-Teller resonance or the $J^\pi=2^-$ component of the spin-flip $\Delta L =1$ resonance as mentioned in Sec. IV F.

B. The Gamow-Teller resonance

Figure 4 displays triton spectra for the Gamow-Teller resonances observed in the Sn(^{3}He,t)Sb reactions at $E(^3\text{He}) = 200$ MeV and $\theta \approx 0°$ on all stable Sn targets. The spectra have been corrected for the contributions from nonresonant background and the $\Delta L = 1$ resonances observed in all Sb isotopes at excitation energies of $E_x = 11$ to 8 MeV above the isobaric analog states. This was done by subtracting the calculated contributions which are shown, for example, in Fig. 2 for ^{118}Sn(^{3}He,t)^{118}Sb. The isobaric analog states are lined up in the figure. The decrease in the relative excitation energies with increasing nucleon number A is apparent. This includes the odd-A nuclei with $A = 117$ and 119 which follow the same trend. The figure clearly shows only one single main Gamow-Teller resonance, and the widths, typically 5–6 MeV, do not change significantly over the range of nuclei from $A = 112$ to 124. The resonances seen are the $T = T_< = T_0-1$ components of the Gamow-Teller resonances. There are no indications for the $T = T_0$ components which are expected ~6 MeV higher in excitation energy.

The excitation energies of the main components of the Gamow-Teller resonances relative to the respective isobaric analog states are displayed in Fig. 5 as function of nucleon number A. The data points from Table II are given as filled circles with error bars of ±250 keV. They decrease with increasing nucleon number and neutron excess, and there is a tendency to asymptotically approach

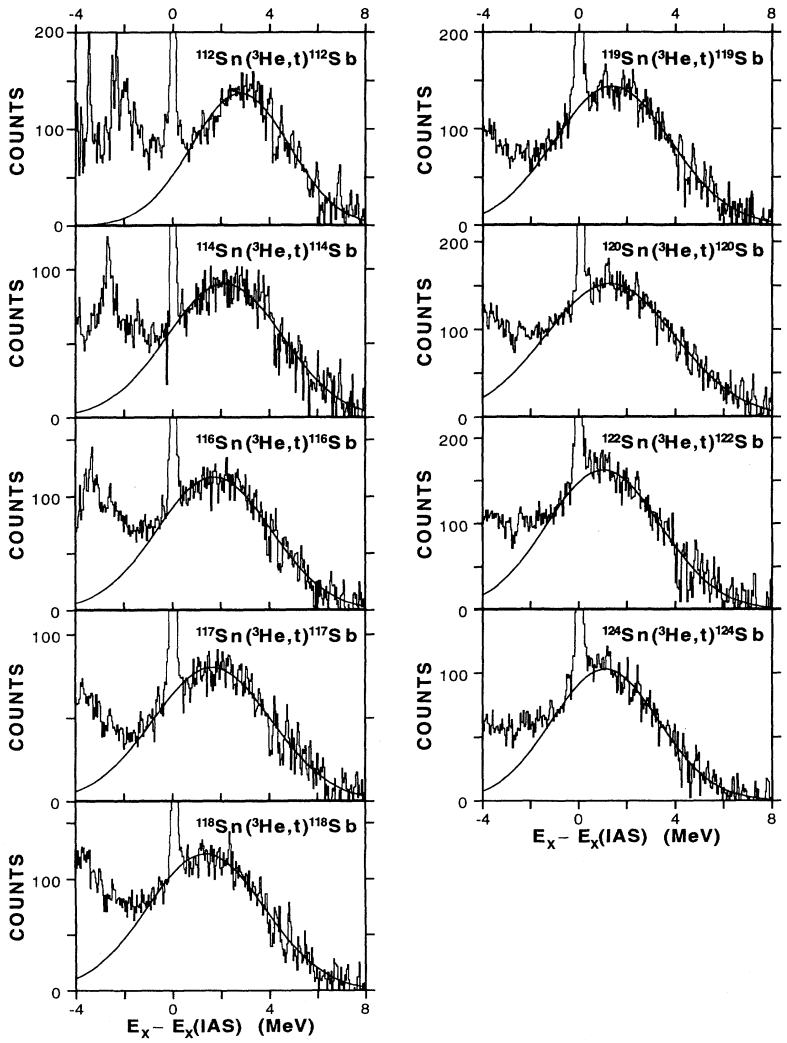

FIG. 4. Corrected triton energy spectra for the main Gamow-Teller resonances observed in ^{A}Sn(^{3}He,t)^{A}Sb on all stable Sn targets. Calculated nonresonant background and the $\Delta L =1$ resonances at higher excitation energies are subtracted.

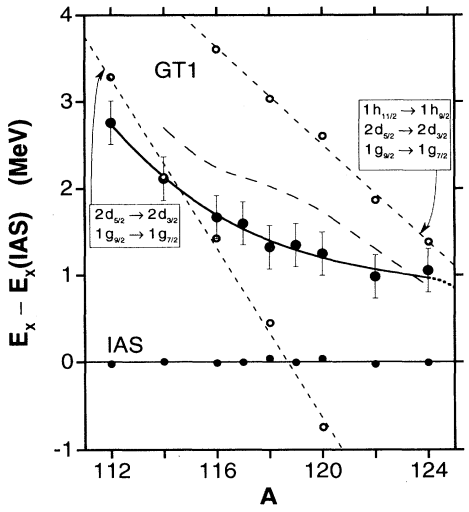

FIG. 5. Differences between the excitation energies of the main component of the Gamow-Teller resonances and the respective isobaric analog states in the Sb isotopes as function of nucleon number A (filled circles). The data are connected by a solid line to guide the eye. Energies for the two calculated components of the main Gamow-Teller resonance [24] (see text) are given as open circles connected by dashed lines. The calculated centroid energies are also given by a dashed line.

the energy of the isobaric analog states. A linear decrease with the asymmetry parameter $(N-Z)/A$ has been considered (e.g., Ref. [11]) to describe a global dependence of these energies from ^{90}Zr to ^{208}Pb. However, the data scatter about the calculated values, and the present data display nonlinear contributions.

Excitation energies have been reported previously based on a few selected Sn(p,n)Sb charge-exchange reactions [11,39], and most excitation energies are slightly higher than measured in the present work by an average of ~260 keV. Furthermore, the (^{3}He,t) reaction has been employed very recently [40] at E(^{3}He) = 450 MeV on several even-A Sn targets, and here the measured excitation energies for the Gamow-Teller resonances also appear to be about 360 keV higher. While almost compatible within the assigned uncertainties, it should be noted, though, that extracted excitation energies are sensitive to the assumed background. Shifts of a few hundred keV are easily possible by assuming a different shape and magnitude for the nonresonant background. Indeed, excitation energies which were even lower by 360 keV and 220 keV than given in Table II were reported [16] for the ^{117,120}Sn(^{3}He,t)^{117,120}Sb reactions, apparently due to the fact that the presence of another weak resonance was assumed above the Gamow-Teller resonance but below the higher-lying $\Delta L = 1$ resonance (see Sec. IV F).

Gamow-Teller resonances represent a coherent superposition of high-lying J^π=1$^+$ proton-particle–neutron-hole configurations of maximum collectivity associated with charge-exchange excitations of neutrons from orbits with $j = \ell + \frac{1}{2}$ into proton orbits with $j = \ell - \frac{1}{2}$ (spin-orbit partner). A close connection between these resonances and isobaric analog states was established theoretically [21,22]. The spin-isospin characteristics of these excitations are related via the Wigner supermultiplet scheme [23]. The energies of the isobaric analog states and the Gamow-Teller resonances should be equal if the Wigner SU(4) symmetry is assumed to be satisfied, and furthermore the resonances would exhaust entirely the respective sum rules. However, already within the shell model, the Wigner SU(4) symmetry is broken by the spin-orbit term of the nuclear mean field. The authors of Refs. [21,22] observed that with increasing asymmetry $(N-Z)/A$ the energy difference between these two excitations becomes small as is well known for ^{208}Bi.

A configuration splitting for the main Gamow-Teller resonances based on the ground states of the Ge and Sn isotopes has been predicted theoretically [24]. For the Sn isotopes, which are considered in the present work, Guba, Nikolaev, and Urin [24] calculated the Gamow-Teller resonances in the framework of the shell optical model taking into account the single-particle continuum, the pairing correlations, and the damping of the Gamow-Teller resonance. All configurations including the one of the orbital with the highest angular momentum, the $1h_{11/2} \rightarrow 1h_{9/2}$ excitation, were considered. Two separate resonances were obtained representing constructive and destructive interference with the $1h_{11/2}$ excitation, and the sum-rule strength becomes distributed between them. The results of this calculation [24] are included in Fig. 5 as two sets of small open circles connected by dashed lines. As the occupation numbers for the $1h_{11/2}$ neutron orbits in the Sn ground states increase, the sum-rule strength shifts from the energetically lower component to the higher component, and a configuration splitting of two collective components separated by ~3 MeV with comparable strengths is predicted near ^{118}Sb at the onset of the filling of the $1h_{11/2}$ neutron orbit. The authors already point out that the experimental observation of configuration splitting is only possible if the total widths Γ are smaller than the predicted splitting ΔE. Otherwise, the effect should be reflected in a variation of the centroid energies of the two resonances. These calculated centroid energies are also included in Fig. 5. The slope differs markedly from those for the two components.

Muraviev and Urin [41] very recently confirmed the effect in an extended calculation generalizing the continuum random-phase-approximation (RPA) approach with the inclusion of neutron pairing and BCS wave functions. The results (not shown) are similar to those displayed in Fig. 5. The two curves deviate somewhat from the dashed lines, particularly for the upper one and for large A, but the calculated centroid energies differ only slightly.

No splitting of the main Gamow-Teller resonance was observed earlier [16] in the investigation of the ^{117,120}Sn(^{3}He,t)^{117,120}Sb reactions, and no such splitting was observed in the present experiment involving all Sn targets. This result may be due to the fact that the total widths of $\Gamma \approx 5-6$ MeV with their estimated uncertainties of ~0.25 MeV exceed the predicted splitting of $\Delta E \approx 3$ MeV. Figure 6(a) includes a bar diagram for the

observed widths Γ of all targets. Despite some scatter, a weak enhancement of the width is indicated in the region $A = 116-120$. This is compatible with an assumed folding of an intrinsic width of $\sim$5 MeV with the predicted splitting of $\sim$3 MeV.

The observed excitation energies of the main Gamow-Teller resonances of Fig. 5 display a transition from the lower to the upper dashed curve as predicted for the calculated centroid energies, but a downward trend at the highest nucleon numbers A is not seen. As noted, the large widths Γ do not permit the observation of the predicted configuration splitting. Nevertheless, the observed A dependence of the excitation energies appears to reflect upon the filling of the $1h_{11/2}$ neutron orbits in the target nuclei, and the data therefore do not contradict the theoretical predictions.

Figure 7(a) includes the cross sections $d\sigma/d\Omega$ at $\theta \approx 0°$ for the main Gamow-Teller resonances GT1. They display a moderate increase with increasing nucleon number and neutron excess. A similar increase for the isobaric analog states is shown in Fig. 7(b). If the validity of the plane-wave or distorted-wave impulse approximations is assumed, and if the reaction mechanisms for the transitions to the main component of the Gamow-Teller resonance and the isobaric analog state are assumed to result from pure charge-exchange spin-flip and non-spin-flip interactions with interaction strengths $V_{\sigma\tau}$ and V_τ, respectively, then the Gamow-Teller and Fermi strengths, $B(\mathrm{GT})$ and $B(F)$, become approximately proportional to the differential cross sections at $\theta = 0°$ [10,12,13]. Using approximations for the energy dependence of kinematic and distortion effects (e.g., Ref. [42]) and assuming $B(F) = N - Z$, it becomes possible to estimate the abso-

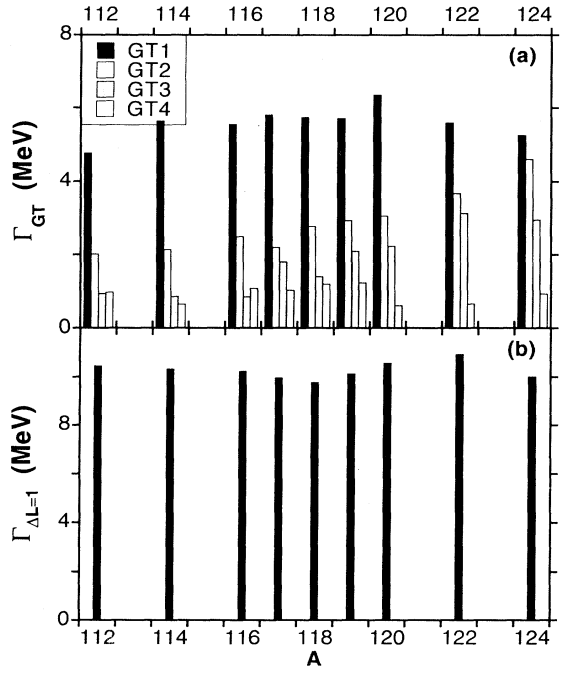

FIG. 6. Total widths Γ for (a) the components of the Gamow-Teller resonances and (b) the $\Delta L = 1$ transitions observed in ^{A}Sn(^{3}He,t)^{A}Sb at $E(^{3}\mathrm{He}) = 200$ MeV on targets with mass numbers $A = 112$, 114, 116, 117, 118, 119, 120, 122, and 124.

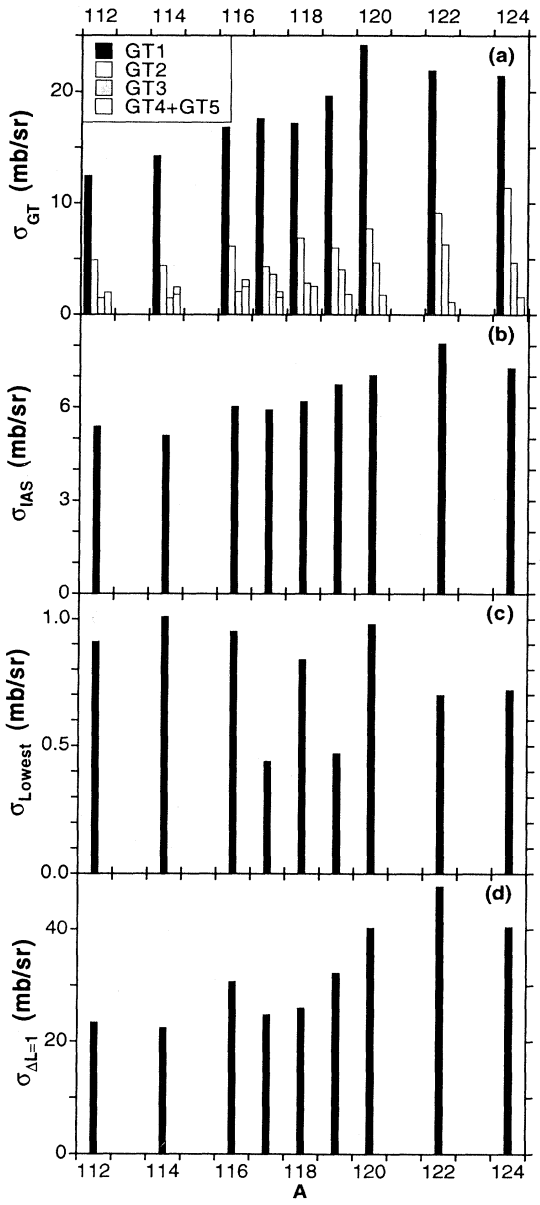

FIG. 7. Cross sections $d\sigma/d\Omega$ measured for the reactions ^{A}Sn(^{3}He,t)^{A}Sb at $E(^{3}\mathrm{He}) = 200$ MeV and $\theta \approx 0°$ leading to (a) the components of the Gamow-Teller resonances, (b) the isobaric analog states, (c) the low-lying $J^\pi = 1^+$ states in the even-A Sb isotopes (or the corresponding $J^\pi = 1/2^+$ states in ^{117,119}Sb), and (d) the $\Delta L = 1$ transitions for targets with nucleon numbers $A = 112$, 114, 116, 117, 118, 119, 120, 122, and 124.

lute Gamow-Teller strengths B(GT). As a result B(GT) for the main component of the Gamow-Teller resonance was found consistently to be about 2/3 of the sum-rule strength of $3(N-Z)$ with an average of $(65 \pm 3)\%$. This result is reasonable considering the expected quenching of the Gamow-Teller strength [43,26,27].

C. "Pygmy" resonances

Figure 8 displays as a function of the nucleon number A the experimental excitation energies (filled circles) of all Gamow-Teller components including the main component GT1 and the "pygmy" resonances GT2, GT3, GT4, (GT5) at lower excitation energies. The energies, also listed in Tables II–IV, were extracted from the results of the fitting procedure as shown in Fig. 2 and the corresponding similar results (not shown) for the other targets. Estimated uncertainties are included. The energies are plotted relative to the adopted energies for the isobaric analog states [34] (open circles). The experimental values for the isobaric analog states shown as open circles deviate from zero by the expected uncertainty of ± 30 keV since they are based on a global energy calibration. The strong $J^\pi = 1^+$ states observed in the even-A isotopes near the ground states (the ground states in ^{118,120}Sb) and the $J^\pi = 1/2^+$ states in the odd-A isotopes are also shown.

Several lines are included in the figure. The heavy dashed line represents the energies of the respective ground states. It displays odd-even staggering due to pairing. The thin dashed lines represent the neutron and proton separation energies of the Sb isotopes. The (upper) neutron line confirms the known fact that isospin-forbidden neutron decay from isobaric analog states is energetically not possible [44] for $A \leq 115$. The (lower) proton line also displays odd-even staggering. Proton decay is energetically not possible below this line, but it is also strongly hindered at excitation energies of 2–3 MeV above this line because of the Coulomb barrier.

The excitation energies relative to the energies of the isobaric analog states show a systematic dependence on nucleon number and neutron excess for all components. This includes both the even-A and the odd-A isotopes. Excluding the sharp "ground states," four "pygmy" resonances each are recorded for A = 114, 116, and 117, and three for the other isotopes. As can be seen from the spectra in Figs. 2 and 3 for ^{118}Sb and is further discussed in Sec. IV D, the characterization of a group of states as members of a resonance is somewhat ambiguous for the very low-lying components below excitation energies of ~2 MeV.

Figure 9 is similar to Fig. 8 with the experimental energies of the Gamow-Teller fragments again plotted as filled circles as a function of A. The solid and dashed lines in this graph represent the early theoretical predictions of Gaponov and Lyutostanskii [21,22] with two slightly different values of the effective coupling constant of the spin-isospin interaction. In addition to the main Gamow-Teller resonances at excitation energies slightly above the isobaric analog states, the authors predicted the possible existence of two low-lying less collective Gamow-Teller fragments on the basis of a quasiclassical treatment within the framework of the random-phase approximation (RPA) [21,22]. The three modes of particle-hole excitations (see, e.g., Fig. 5 in Ref. [16]) were charac-

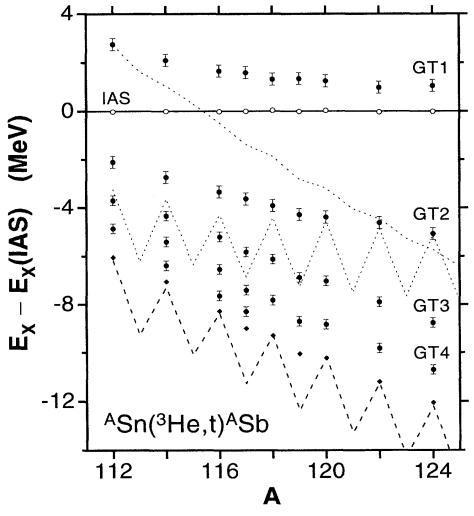

FIG. 8. Experimental excitation energies relative to the isobaric analog states of the components GT1 to GT4 (or GT5) of the Gamow-Teller resonances (filled circles) as function of nucleon number A. The low-lying $J^\pi = 1^+$ states in the even-A nuclei and $J^\pi = 1/2^+$ states in the odd-A isotopes are also shown (filled diamonds). The heavy dashed line represents the energies $E_{g.s.}$ of the respective ground states. The thin dashed lines represent the energies below which neutron and proton emission are energetically not possible.

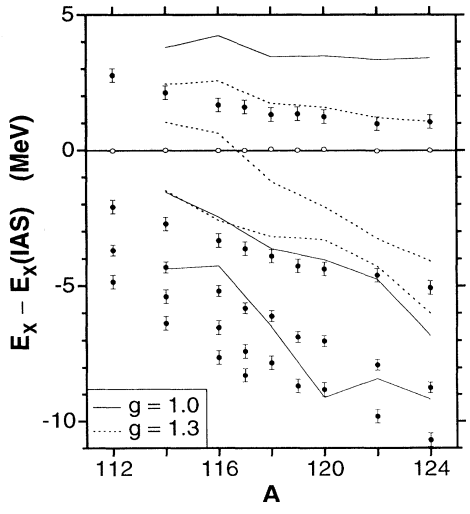

FIG. 9. Experimental excitation energies as in Fig. 8. Here, the solid and dashed lines represent the theoretical predictions of Refs. [21,22] (see text) for the semiclassical direct-, core-polarization-, and back-spin-flip Gamow-Teller resonances.

terized as direct spin flip ($j = \ell + \frac{1}{2} \rightarrow j = \ell - \frac{1}{2}$), core-polarization spin flip ($j = \ell \pm \frac{1}{2} \rightarrow j = \ell \pm \frac{1}{2}$), and back spin flip ($j = \ell - \frac{1}{2} \rightarrow j = \ell + \frac{1}{2}$). Whereas there is only moderate quantitative agreement between the three sets of calculated curves shown in Fig. 9 and the experimental data, the general trends are already quite well predicted.

There exist only two weak Gamow-Teller fragments within the framework of this simplified shell-model treatment (three-level model) [21,22,24]. Fragmentation into three or more low-lying slightly collective states of the particle-hole type has been predicted by several authors (e.g., Refs. [25–28,45]) using a variety of approaches including the RPA within the quasiparticle-phonon model, with the use of a realistic particle-hole basis, or with a strongly nonlocal residual interaction. The number of states depends on the number of discrete and quasidiscrete Gamow-Teller particle-hole configurations. Theoretical spectra with three or four lower-lying fragments [26,28,16] are indeed reported for the Sn isotopes in agreement with the data.

The relative Gamow-Teller strengths of the "pygmy" resonances for the Sn isotopes were estimated by Gaponov and Lyutostanskii [21,22] to range from 10% (^{114}Sb) to 25% (^{124}Sb). In a recent reevaluation of the three-level model [45] it was found that these values may be overestimated by a factor of ~ 2. On the other hand, average strengths of 26% for targets of ^{120}Sn and ^{124}Sn were also reported [26].

Figure 7(a) includes the 0° cross sections for all components of the Gamow-Teller resonances. The cross sections for the "pygmy" resonances increase with increasing neutron excess, but they are significantly smaller than those for the main components. Combining the cross sections with the ones for the isobaric analog states given in Fig. 7(b) to extract Gamow-Teller strength B(GT) immediately showed, as already observed earlier [16], that B(GT) is overestimated for these resonances with their reduced collectivity. This effect is particularly apparent for the J^π=1$^+$ ground states in ^{118}Sb and ^{120}Sb where the B(GT) values so extracted exceed those deduced from the known log(ft) values from the β^+ decay by a factor of ~ 5. A quantitative comparison between the present data and theoretically predicted B(GT) values is therefore not yet possible.

It is concluded that these lower J^π=1$^+$ resonances and states must contain admixtures probably from ΔL =2 spin-flip configurations which can be excited at our bombarding energy via the tensor interaction. Since the occupation numbers for the $2d_{5/2}$ and $1g_{7/2}$ neutron orbits are close to unity for most of the Sn ground states, particle-hole configurations of the type $(2d_{5/2})(1g_{7/2})^{-1}$ and $(1g_{7/2})(2d_{5/2})^{-1}$ are likely candidates. Whereas ΔL =0 spin-flip transitions mediated by the central interaction $V_{\sigma\tau}$ lead to the excitation of the regular particle-hole Gamow-Teller components, ΔL =2 spin-flip transitions mediated by the noncentral tensor interaction $V_{T\tau}$ contribute to the cross sections, even at $\theta = 0°$, due to the presence of such ΔL =2 spin-flip contributions. The enhanced cross sections are the result of constructive interference between the Gamow-Teller and "L-forbidden" Gamow-Teller transitions. They make the observation of the "pygmy" resonances possible. A quantitative verification of this behavior has to await information about the strengths of the effective interactions $V_{\sigma\tau}$ and $V_{T\tau}$.

The cross sections for the "pygmy" resonances of Fig. 7(a) increase by a factor of $\sim$2 over the range A = 112 to 124. The widths Γ of Fig. 6(a) increase as well by a similar factor. Therefore, the "pygmy" resonances appear more prominent for low nucleon numbers A where the resonances are significantly sharper.

D. Substructures and doorway states

Triton energy spectra for all ^{A}Sn(^{3}He,t)^{A}Sb reactions measured at $\theta \approx 0°$ are displayed in Fig. 10 for low excitation energies up to E_x = 8 MeV with an energy binning of 40 keV/channel. The spectra are lined up at the ground states. The energy spectra for the two odd-A targets ^{117}Sn and ^{119}Sn are included but shifted by 2.3 MeV to approximately align the strong J^π=1$^+$ low-lying states in the even-A isotopes and the respective J^π =1/2$^+$ states in the odd-A isotopes.

The spectra display numerous discrete states. These states are clustered together, and they are correlated with the low-lying "pygmy" resonances as indicated in the figure and discussed in the previous Sec. IV C. The fine structure is most pronounced at the lowest excitation energies, but it is more difficult below excitation energies of $\sim$2 MeV to correlate the structures with particular resonances. Levels identified by ΔL = 0 transitions (from the 0° and 2° cross sections) are labeled by their excitation energies or short vertical markers. The main component of the Gamow-Teller resonances does not display fine structure.

All states observed in the Sb isotopes are believed to have J^π=1$^+$ for even-A or J^π =(1/2, 3/2)$^+$ for odd-A nuclei. In fact, all *known* low-lying states [35] with excitation energies close to the ones observed in the present work (given in Table VIII) have these spin-parity assignments. This includes the five lowest states observed in ^{116}Sb and the ground states of ^{118,120}Sb.

States with J^π=0$^+$ in the Sb nuclei with excitation energies below the isobaric analog states cannot be strongly excited. Antianalog states are expected to be present at these low excitation energies. However, they cannot be populated by the $T^- = \sum \tau_i^-$ operator which is responsible for the coherent collective excitation of the isobaric analog states. The T_0−1 component of the isovector monopole resonance, which is excited via the operator $\sum r_i^2 \tau_i^-$, can admix via the strong interaction into the $T = T_0 - 1$, $T_z = T_0 - 1$ antianalog states. However, very little isovector monopole strength is expected to be moved down to these low excitation energies. Therefore, no strong excitation of low-lying J^π=0$^+$ antianalog states can be expected from this mixing mechanism.

The observed substructures are believed to be the result of mixing of the various Gamow-Teller one-particle–one-hole (1p-1h) components with 2p-2h doorway states with J^π=1$^+$. The structures are most pronounced at the lowest excitation energies where the level densities are

the lowest. Beginning at excitation energies of ~4 MeV the states seem to overlap. The substructures gradually disappear at higher excitation energies, and essentially no structures are seen for the main Gamow-Teller components.

The density of these doorway states increases only weakly with excitation energy. This effect is known from the investigation of the spreading widths $\Gamma^{\downarrow}$ of isobaric analog states [46]. In the simple picket-fence model the spreading widths $\Gamma^{\downarrow}$ are proportional to the density of doorway states. The widths $\Gamma^{\downarrow}$ for the isobaric analog states increase for E_x = 10 to 20 MeV by not more than a factor of ~10, or by a factor of ~2 for an increase in excitation energy of a little over 3 MeV. This can be approximated by an exponential dependence on excitation energy, and the increase is many orders of magnitude weaker [46] than the increase in the level density of all states with the same spin and parity expected from level-density formulas.

An inspection of the spectra of Fig. 10 makes it possible to establish an estimate for the number of $J^{\pi}=1^{+}$ doorway states. Quite clearly, here again, the density increases much less rapidly than the density of all states with the same J^{π}. Keeping in mind that some of the over-

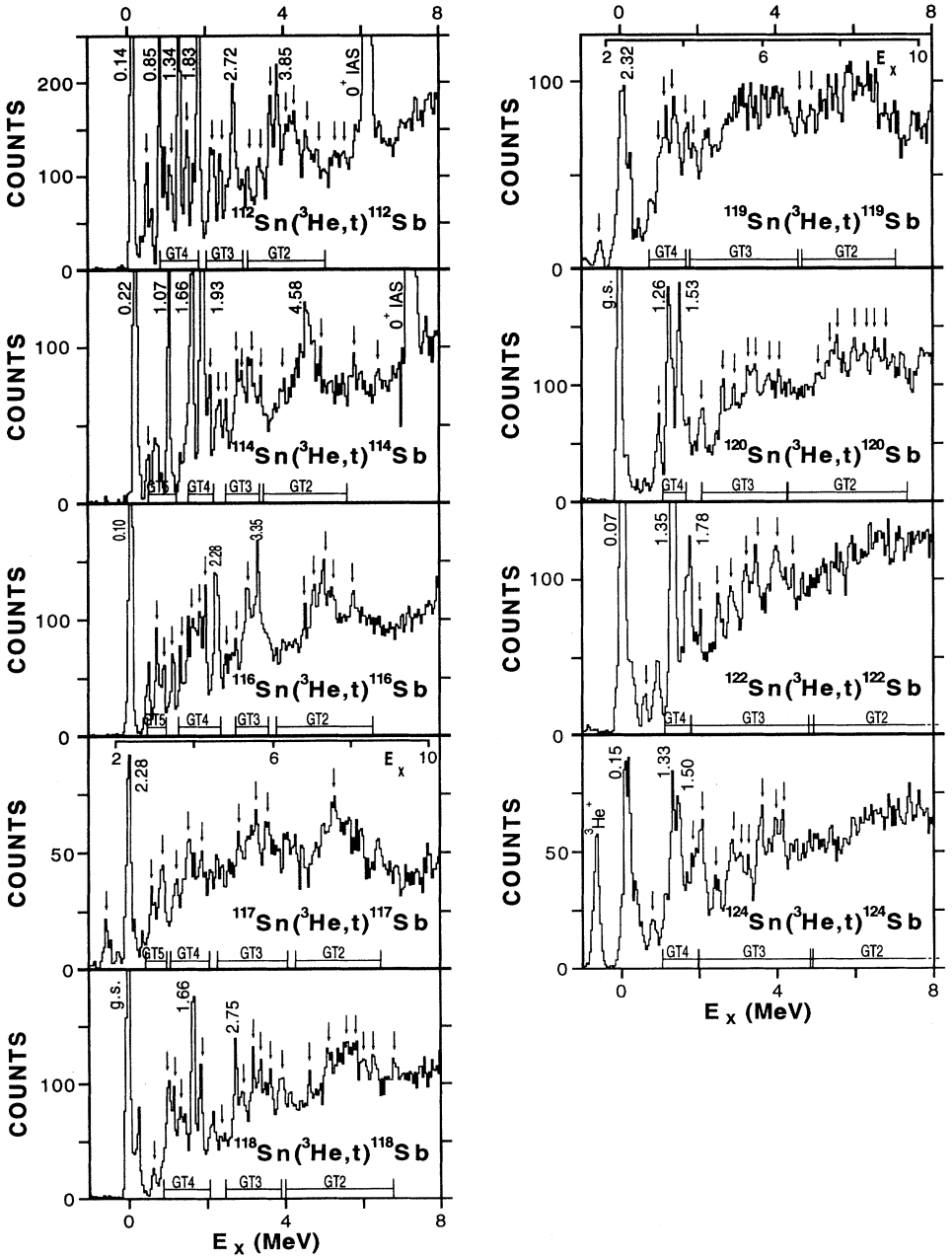

FIG. 10. Triton energy spectra for the ^{A}Sn(^{3}He,t)^{A}Sb reactions at $E(^{3}\mathrm{He})$ = 200 MeV and $\theta \approx 0°$ for A =112, 114, 116, 117, 118, 119, 120, 122, and 124. The measured momentum spectra are linearized in energy and cover the regions of low excitation energies up to E_x = 8 MeV with an energy binning of 40 keV/channel. The spectra are lined up in excitation energy except for the two odd-A targets ^{117}Sn and ^{119}Sn which are shifted by 2.3 MeV. All ΔL = 0 transitions are labeled by their excitation energies or vertical markers.

lapping levels are not resolved above $E_x \approx 4$ MeV, one can estimate level densities of ~3.5/MeV and ~7/MeV for excitation energies of ~2 MeV and ~5 MeV, respectively. Interestingly, this increase is similar to that required in the explanation of the spreading widths $\Gamma^{\downarrow}$ of the isobaric analog states at higher excitation energies. This result supports the interpretation of these states as 2p-2h doorway states. The extrapolation of the present estimate yields doorway level densities of 20/MeV to 40/MeV for the main Gamow-Teller resonances. This explains why no substructures are observed there.

As mentioned above, neutron and proton emission are energetically not possible from the pygmy resonances and their associated doorway states.

E. The $J^\pi = 1^+$ "ground states"

The excitation energies relative to the isobaric analog states for the energetically lowest states in the Sb isotopes with $\Delta L = 0$ transitions have been included in Fig. 8. The $J^\pi=1^+$ states in the even-A isotopes follow an almost straight line very close to the respective ground states ($E_x \leq 220$ keV), and in ^{118,120}Sb they are in fact the ground states. The energies for the corresponding odd-A isotopes follow almost the same trend except that their energies (relative to the isobaric analog states) are 200–250 keV lower than the average of their even-A neighbors. Because of odd-even staggering the excitation energies in ^{117,119}Sb relative to the ground states are ~2.3 MeV.

It appears that the nuclear structure of these states must be similar. This is supported by the cross sections for the transitions to the $J^\pi=1^+$ states which are essentially equal, ~0.9 mb/sr [see Fig. 7(c)]. From the known log(ft) values of the ground state β^+ decays of ^{118,120}Sb(1^+) $\rightarrow^{118,120}$ Sn(0^+) with log(ft) = 4.5 [35], B(GT) values for Sn $\rightarrow$ Sb can be calculated. It follows that only ~20% of the observed (^{3}He,t) charge-exchange transition strength is due to ΔL =0 spin-flip mediated by the central interaction $V_{\sigma\tau}$, while ~80 % is due to ΔL =2 spin-flip mediated by the noncentral tensor interaction $V_{T\tau}$. As mentioned in Sec. IV D, the $2d_{5/2}$ and $1g_{7/2}$ neutron orbits in the Sn ground states have high occupation numbers of typically ~90 %. Therefore, particle-hole configurations of the type $(2d_{5/2})(2d_{5/2})^{-1}$ and $(1g_{7/2})(1g_{7/2})^{-1}$ are likely components responsible for ΔL =0 spin flip, and particle-hole configurations of the type $(2d_{5/2})(1g_{7/2})^{-1}$ and $(1g_{7/2})(2d_{5/2})^{-1}$ are likely components for ΔL =2 spin flip. The observed strong $J^\pi=1^+$ "ground states" presumably represent a coherent superposition of strength from Gamow-Teller and "L-forbidden" Gamow-Teller transitions. This conjecture is supported by the fact that many states with $J^\pi=1^+$ up to $J^\pi=6^+$ are observed [35] as low-lying states in the Sb isotopes.

An additional question arises about the structure of the corresponding states observed in the odd-A isotopes of Sb. If one assumes that the $2s_{1/2}$ neutron in the ground states of ^{117,119}Sn acts as a spectator, then the weak coupling to the $J^\pi=1^+$ configuration should lead to a J^π =($1/2^+$,$3/2^+$) doublet with an intensity ratio of 1 to 2. However, only a single state is observed in both ^{117}Sb and ^{119}Sb. (There is a doublet seen in ^{119}Sb, but only one of the two states is from a ΔL =0 transition.) Furthermore, the state observed in ^{117}Sb at E_x = 2280 keV can be identified with a known J^π =$1/2^+$ state at E_x = 2285 keV [35] (see Table VIII). Hence, there is only one component present with J^π =$1/2^+$. The origin and structure of this state is unknown. Another interesting result [see Fig. 7(c)] is the fact that the cross sections for the transitions to the J^π =$1/2^+$ states are on the order of 50% of those for the $J^\pi=1^+$ states. This behavior is not explained, but it is reminiscent of Pauli blocking of $s_{1/2}$ neutron orbitals as observed in (p,t) two-nucleon transfer [47] and (d,α) four-nucleon transfer reactions [48].

F. Resonances with $\Delta L = 1$

The triton spectra for ^{118}Sn(^{3}He,t)^{118}Sb of Fig. 2 show a broad resonance at E_x = 18.7 MeV or 9.4 MeV above the isobaric analog state. Unlike the Gamow-Teller transitions which display a very strong forward enhancement, this transition has a weak minimum at 0°. It is therefore identified with $\Delta L \geq 1$, most likely $\Delta L = 1$.

The observed centroid energies for these resonances on all Sn targets are displayed in Fig. 11, and their widths Γ and cross sections $d\sigma/d\Omega(0°)$ are shown in the previous bar diagrams of Figs. 6(b) and 7(d), respectively. The excitation energies relative to the isobaric analog states decrease strongly with increasing neutron excess from ~10.8 to ~8.3 MeV. The widths are essentially constant, $\Gamma \approx 9$ MeV, and the 0° cross sections increase slowly with neutron excess. Data for ΔL =1 resonances have been observed independently [11,40] on selected Sn tar-

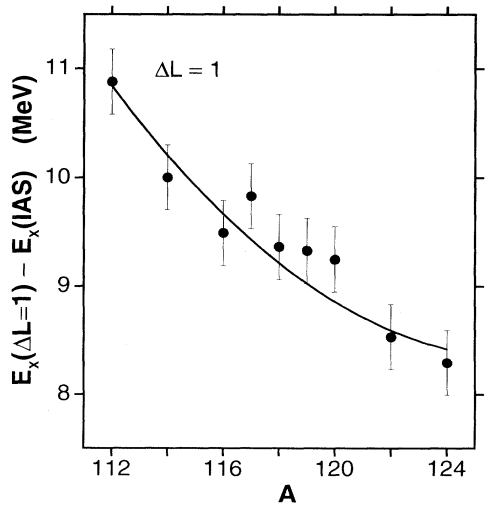

FIG. 11. Excitation energies for the ΔL = 1 resonances observed in the Sb isotopes as function of nucleon numbers A. The solid line is included to guide the eye.

gets for (p,n) and (^{3}He,t) at higher bombarding energies per nucleon. The excitation energies observed in these experiments are slightly lower, typically by ~300 keV, but almost still within the shown uncertainties.

The resonances observed in the present work presumably represent an incoherent superposition of the $T_<$ components of the non-spin-flip and spin-flip $\Delta L = 1$ resonances with $J^\pi = 1^-$ and also the $\Delta L = 1$ spin-flip transitions with $J^\pi = 2^-$ and $J^\pi = 0^-$. Both non-spin-flip and spin-flip $\Delta L = 1$ resonances are expected to be strongly populated at our bombarding energy. The resonances observed at the higher bombarding energies, however, should represent essentially pure spin-flip $\Delta L = 1$ resonances. It therefore appears that the non-spin-flip and spin-flip resonances have similar excitation energies. Such a close degeneracy between the giant dipole and spin-dipole resonances is known, for example, in ^{12}N and ^{12}B (see Refs. [49,50]).

Uncertainties enter into the determination of excitation energies as mentioned above because in addition to the $J^\pi = 1^-$ component of the spin dipole resonance there must exist $J^\pi = 2^-$ and 0^- components at energies of typically 2 MeV below and 4 MeV above the $J^\pi = 1^-$ component (e.g., Ref. [51]). The presence of a $J^\pi = 2^-$ resonance was assumed in the analysis of the earlier data for ^{117,120}Sn [16], and the reported excitation energies are indeed slightly shifted. It should also be noted that a weak component of the Gamow-Teller resonance with $T = T_0$ is expected about 6 MeV above the main Gamow-Teller resonance, which, if not included, could also contribute to an apparent shift of the observed higher $\Delta L = 1$ resonances.

G. Nonresonant background

The triton spectra for ^{118}Sn(^{3}He,t)^{118}Sb of Fig. 2 display a calculated continuous nonresonant background. This background is based on the quasifree charge-exchange reaction on bound neutrons, $n_{bound}(^3He,t)p_{free}$. The removal of a proton leaves the residual nucleus in its ground state or an excited single-neutron hole state. The Fermi motion of the neutron which interacts with the projectile leads to a significant energy broadening. The onset of the continuum is determined by the threshold for the respective three-body breakup. A good analytical description of this effect is given [37,38] by the equation

$$\frac{d^2\sigma}{dEd\Omega} = N_0 \frac{1-\exp[(E_t - E_0)/T]}{1+[(E_t - E_{QF})/W]^2}. \quad (1)$$

This simple analytical expression has been successfully used in pion-induced charge-exchange reaction. The centroid energy E_{QF} is shifted relative to the energy E_t(free) of the free process, $n_{free}(^3He,t)p_{free}$, by the proton binding energy S_p, the excitation energy $E_x^{(n)}$ of the neutron-hole state, and the Coulomb barrier B_{Coul} for the proton, hence $E_{QF} = E_t(\text{free}) - (S_p + E_x^{(n)} + B_{Coul})$. The energy $E_x^{(n)}$ is zero only if the neutron is removed from the orbit nearest the Fermi surface. The width W is due to the Fermi motion. The exponential term is due to Pauli blocking, and the quantity T has the characteristics of a temperature. The cutoff energy $E_0 = E_t(\text{g.s.}) - S_p$ is determined by the three-body breakup energy and was fixed at these values in the present calculation. The width parameters T and W were fixed at predetermined values of $T = 100$ MeV and $W = 22$ MeV (for more details see Ref. [16]). Only the quantities E_{QF} and N_0 were used in the fitting procedure as adjustable parameters. The extracted values for the centroid energies E_{QF} are very stable for the nine fits for the different isotopes and range from 177 to 182 MeV. The amplitudes N_0 have been used to extract cross sections for the quasifree charge-exchange process as discussed next.

It can be seen from the triton spectra of Fig. 2 that, as expected, the cross sections for the quasifree charge-exchange process change only very little over the angular range from 0° to 2°. In addition, the measured cross sections make it possible to estimate the fraction of participating valence neutrons. The above equation, with the parameters extracted from the fitting procedure, yield cross sections for the quasi-free process. The free charge-exchange reaction ^{3}He$(n,p)^3$H has been measured very recently [52] at essentially the same c.m. bombarding energy as in the present experiment. The differential cross section at $\theta = 0°$ is ~20 mb/sr. The ratio of the respective cross sections is shown in Fig. 12 as function of nucleon number A. It represents the number of neutrons which participate in the quasifree process at our bombarding energy. This number increases systematically with nucleon number and neutron excess from ~12 to ~17 neutrons. However, this increase is less rapid than that for the neutron excess $N - Z$ which is also shown in Fig. 12. The fraction of participating neutrons to the number of valence neutrons (excess neutrons) decreases from 100 to 70%, and the average fraction is ~85%. The

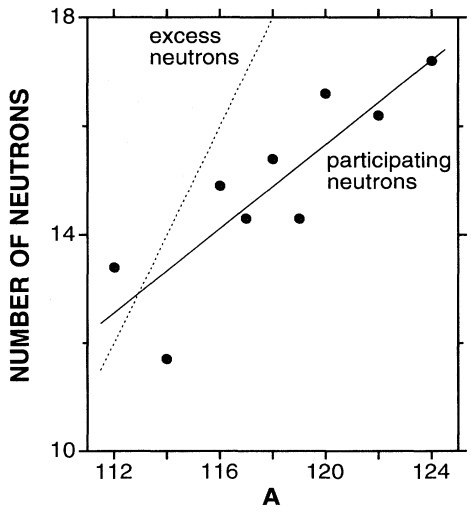

FIG. 12. Number of participating neutrons in the quasifree charge-exchange process as function of nucleon number A derived from the measured cross sections. The number of valence neutrons (neutron excess) is shown by a dashed line.

agreement with the occupation probabilities observed in electron-induced proton knockout from valence shells [53] of ~70% is quite satisfactory given the uncertainties of the present cross sections and the observed strong variation with neutron excess.

V. SUMMARY

A comprehensive study of the (^{3}He,t) charge-exchange reaction on essentially all stable Sn isotopes has been performed at $E(^3\text{He})$=200 MeV near $\theta = 0°$. Triton energy spectra were obtained with high energy resolution up to excitation energies of ~28 MeV. The differences of the spectra measured simultaneously at $\theta \approx 0°$ and $\theta \approx 2°$ are very sensitive to transitions with $\Delta L = 0$ because they are strongly peaked at 0°. The main Gamow-Teller resonances are strongly excited with ~65 % of the sum-rule strength of $3(N - Z)$. The dependence on nucleon number A of the excitation energies reflects upon the filling of the $1h_{11/2}$ neutron orbit in the Sn target nuclei. A theoretically predicted configuration splitting of these resonances could not be observed, possibly due to the fact that the total widths Γ exceed the predicted splitting.

Also excited are several Gamow-Teller fragments at lower excitation energies ("pygmy" resonances). Interference between the transition strengths of ΔL =0 spin flip, mediated by the central interaction $V_{\sigma\tau}$, and ΔL =2 spin flip, mediated by the noncentral tensor interaction $V_{T\tau}$, enhances the cross sections for these low-lying particle-hole components. Furthermore, the low-lying resonances were found to display pronounced fine structures of J^π=1^+ states which are interpreted as 2p-2h doorway states. The density of these doorway states increases slowly with excitation energy. A systematic sequence of J^π=1^+ states at or near the ground states is strongly excited for all even-A Sb isotopes as are J^π =$1/2^+$ states in ^{117,119}Sb at corresponding excitation energies.

Nonresonant quasifree charge exchange was observed with cross sections increasing with neutron excess reflecting upon the increase in the number of participating neutrons. A fraction of ~85 % of all excess neutrons was found to participate in this process in approximate agreement with electron-induced proton knockout data.

ACKNOWLEDGMENTS

The authors acknowledge helpful discussions with M. H. Urin, S. E. Muraviev, K. T. Hecht, and B. A. Brown and the support provided by the technical staff of the Indiana University Cyclotron Facility, in particular by C. C. Foster and W. R. Lozowski. The research was supported in part by National Science Foundation Grants No. PHY-9208468 (UM, Ann Arbor) and No. PHY-9314783 (IUCF). The travel Grants No. 85-0123 and No. 90-0219 provided by the Scientific Affairs Division, North Atlantic Treaty Organization, are gratefully acknowledged.

[1] C. Gaarde, K. Kemp, Y. V. Naumov, and P. R. Amundson, Nucl. Phys. **A143**, 497 (1970).
[2] C. Gaarde, K. Kemp, C. Petresch, and F. Folkmann, Nucl. Phys. **A184**, 241 (1972).
[3] C. Gaarde and T. Kammuri, Nucl. Phys. **A215**, 314 (1973).
[4] W. R. Wharton and P. D. Debevec, Phys. Lett. **51B**, 447 (1974); Phys. Rev. C **11**, 1963 (1975).
[5] A. Galonsky, R. R. Doering, D. M. Patterson, and H. W. Bertini, Phys. Rev. C **14**, 748 (1976).
[6] R. R. Doering, A. Galonsky, D. M. Patterson, and G. F. Bertsch, Phys. Rev. Lett. **35**, 1691 (1975).
[7] M. B. Blann, R. R. Doering, A. Galonsky, D. M. Patterson, and F. E. Serr, Nucl. Phys. **A257**, 15 (1976).
[8] W. A. Sterrenburg, S. M. Austin, U. E. P. Berg, and R. DeVito, Phys. Lett. **91B**, 337 (1980).
[9] D. E. Bainum, J. Rapaport, C. D. Goodman, D. J. Horen, C. C. Foster, M. B. Greenfield, and C. A. Goulding, Phys. Rev. Lett. **44**, 1751 (1980).
[10] C. D. Goodman, C. A. Goulding, M. B. Greenfield, J. Rapaport, D. E. Bainum, C. C. Foster, W. G. Love, and F. Petrovitch, Phys. Rev. Lett. **44**, 1755 (1980).
[11] D. J. Horen, C. D. Goodman, C. C. Foster, C. A. Goulding, M. B. Greenfield, J. Rapaport, D. E. Bainum, E. Sugarbaker, T. G. Masterson, F. Petrovitch, and W. G. Love, Phys. Lett. **95B**, 27 (1980).
[12] T. N. Taddeucci, J. Rapaport, D. E. Bainum, C. D. Goodman, C. C. Foster, C. Gaarde, J. Larsen, C. A. Goulding, D. Horen, T. Masterson, and E. Sugarbaker, Phys. Rev. C **25**, 1094 (1981).
[13] T. N. Taddeucci, C. A. Goulding, T. A. Carey, R. C. Byrd, C. D. Goodman, C. Gaarde, J. Larsen, D. Horen, J. Rapaport, and E. Sugarbaker, Nucl. Phys. **A469**, 125 (1987).
[14] H. J. Hofmann, S. Brandenburg, P. Grasdijk, M. N. Harakeh, W. A. Sterrenburg, and S. Y. van der Werf, Nucl. Phys. **A433**, 181 (1985).
[15] J. Jänecke, F. D. Becchetti, A. M. van den Berg, G. P. A. Berg, G. Brower, M. B. Greenfield, M. N. Harakeh, M. A. Hofstee, A. Nadasen, D. A. Roberts, R. Sawafta, J. M. Schippers, E. J. Stephenson, D. P. Stewart, and S. Y. van der Werf, Nucl. Phys. **A526**, 1 (1991).
[16] J. Jänecke, K. Pham, D. A. Roberts, D. Stewart, M. N. Harakeh, G. P. A. Berg, C. C. Foster, J. E. Lisantti, R. Sawafta, E. J. Stephenson, A. M. van den Berg, S. Y. van der Werf, S. E. Muraviev, and M. H. Urin, Phys. Rev. C **48**, 2828 (1993).
[17] H. Akimune, I. Daito, Y. Fujita, M. Fujiwara, M. B. Greenfield, M. N. Harakeh, T. Inomata, J. Jänecke, K. Katori, S. Nakayama, H. Sakai, Y. Sakemi, M. Tanaka, and M. Yosoi, Nucl. Phys. **A569**, 245c (1994).
[18] H. Akimune, I. Daito, Y. Fujita, M. Fujiwara, M. B. Greenfield, M. N. Harakeh, T. Inomata, J. Jänecke, K. Katori, S. Nakayama, H. Sakai, Y. Sakemi, M. Tanaka, and M. Yosoi, Nucl. Phys. **A569**, 255c (1994).
[19] H. Akimune, I. Daito, Y. Fujita, M. Fujiwara, M. B. Greenfield, M. N. Harakeh, T. Inomata, J. Jänecke, K. Katori, S. Nakayama, H. Sakai, Y. Sakemi, M. Tanaka,

and M. Yosoi, Phys. Lett. B **323**, 107 (1994).
[20] K. Ikeda, S. Fujii, and J. I. Fujita, Phys. Lett. **3B**, 271 (1963); J. I. Fujita and K. I. Ikeda, Nucl. Phys. **67**, 145 (1965).
[21] Yu. V. Gaponov and Yu. S. Lyutostanskii, Yad. Fiz. **19**, 62 (1974) [Sov. J. Nucl. Phys. **19**, 33 (1974)].
[22] Yu. V. Gaponov and Yu. S. Lyutostanskii, Fiz. Elem. Chastits At. Yadra **12**, 1324 (1981) [Sov. J. Part. Nucl. **12**, 528 (1981)].
[23] E. P. Wigner, Phys. Rev. **51**, 106 (1937); **56**, 519 (1939).
[24] V. G. Guba, M. A. Nikolaev, and M. H. Urin, Phys. Lett. B **218**, 283 (1989).
[25] K. Grotz, H. V. Klapdor, J. Metzinger, R. Madey, W. Parsuwan, B. D. Anderson, A. R. Baldwin, B. Flanders, C. Lebo, J. W. Watson, and C. C. Foster, Phys. Lett. **126B**, 417 (1983).
[26] V. A. Kuzmin and V. G. Soloviev, J. Phys. G **10**, 1507 (1984).
[27] V. A. Kuzmin, Joint Institute for Nuclear Research Report No. JINR P4-93-449, 1993 (in Russian); in International Conference on Selected Topics in Nuclear Structure, Dubna, Russia, 1994 (JINR Report No. E4-94-168, 1994), p. 69.
[28] M. H. Urin (private communication).
[29] J. Jänecke, in International Conference on Nuclear Structure and Nuclear Reactions at Low and Intermediate Energies, Dubna, Russia, 1992 (JINR Report No. E4-93-58, 1993), p. 303.
[30] J. Jänecke *et al.*, in International Conference on Selected Topics in Nuclear Structure, Dubna, Russia, 1994 (JINR Report No. E4-94-168, 1994), p. 56.
[31] G. P. A. Berg, L. C. Bland, B. M. Cox, D. DuPlantis, D. W. Miller, K. Murphy, P. Schwandt, K. A. Solberg, E. J. Stephenson, B. Flanders, and H. Seifert, IUCF Scientific and Technical report, 1986 (unpublished), p. 152.
[32] G. P. A. Berg, L. C. Bland, D. DuPlantis, C. C. Foster, D. W. Miller, P. Schwandt, R. Sawafta, K. A. Solberg, and E. J. Stephenson, IUCF Scientific and Technical report, 1987-88 (unpublished), p. 233.
[33] IUCF Internal report: XSYS Data Acquisition Software (May 1988, revised April 1990). The original version was developed at Triangle Universities Nuclear Laboratory (TUNL).
[34] M. S. Antony, J. Britz, and A. Pape, At. Data Nucl. Data Tables **40**, 9 (1988).
[35] NNDC Online Data Service, National Nuclear Data Center, Brookhaven National Laboratory, Upton, New York; funded by the U.S. Department of Energy, Office of Energy Research, Division of Nuclear Physics.
[36] K. Dennis, H. Akimune, G. P. A. Berg, S. Chang, B. Davis, M. Fujiwara, M. N. Harakeh, J. Jänecke, J. Liu, K. Pham, D. A. Roberts, and E. J. Stephenson, Phys. Rev. A **50**, 3992 (1994).
[37] A. Erell, J. Alster, J. Lichtenstadt, M. A. Moinester, J. D. Bowman, M. D. Cooper, F. Irom, H. S. Matis, E. Piasetzki, and U. Sennhauser, Phys. Rev. C **34**, 1822 (1986); A. Erell, Ph.D. thesis, Tel-Aviv University, 1984 (unpublished).
[38] F. Irom, J. D. Bowman, G. O. Bolme, E. Piastzky, U. Sennhauser, J. Alster, J. Lichtenstadt, M. Moinester, J. N. Knudson, S. H. Rokni, and E. R. Siciliano, Phys. Rev. C **34**, 2231 (1986).
[39] B. D. Anderson, B. S. Flanders, C. Lebo, R. Madey, and J. W. Watson, in Ref. [29], p. 227.
[40] M. Fujiwara (private communication).
[41] S. E. Muraviev and M. H. Urin, in Ref. [30], p. 78.
[42] B. S. Flanders, R. Madey, B. D. Anderson, A. R. Baldwin, J. W. Watson, C. C. Foster, H. V. Klapdor, and K. Grotz, Phys. Rev. C **40**, 1985 (1989).
[43] F. Osterfeld, Rev. Mod. Phys. **64**, 491 (1992), and references therein.
[44] J. Jänecke, J. A. Bordewijk, S. Y. van der Werf, and M. N. Harakeh, Nucl. Phys. **A552**, 323 (1993).
[45] V. G. Guba, M. A. Nikolaev, and M. G. Urin, Yad. Fiz. **51**, 973 (1990) [Sov. J. Nucl. Phys. **51**, 662 (1990)].
[46] J. Jänecke, M. N. Harakeh, and S. Y. van der Werf, Nucl. Phys. **A463**, 571 (1987).
[47] D. G. Fleming, M. Blann, and H. W. Fulbright, Nucl. Phys. **A163**, 401 (1971).
[48] F. D. Becchetti and J. Jänecke, Phys. Rev. Lett. **35**, 268 (1975).
[49] S. Nakayama, T. Yamagata, M. Tanaka, M. Inoue, K. Yuassa, T. Itahashi, H. Ogata, N. Koori, K. Shima, and M. B. Greenfield, Phys. Rev. C **46**, 1667 (1992).
[50] C. Gaarde, J. Rapaport, T. N. Taddeucci, C. D. Goodman, C. C. Foster, D. E. Bainum, C. A. Goulding, M. B. Greenfield, D. J. Horen, and E. Sugarbaker, Nucl. Phys. **A369**, 258 (1981).
[51] V. A. Kuzmin and V. G. Soloviev, J. Phys. G **11**, 603 (1985).
[52] A. Celler, S. Yen, W. P. Alford, R. Abegg, B. A. Brown, S. Burzynski, D. Frekers, O. Häusser, R. Helmer, R. S. Henderson, K. Hicks, K. P. Jackson, R. Jeppesen, C. A. Miller, M. A. Moinester, B. W. Pointon, A. Trudel, and M. C. Vetterli, Phys. Rev. C **47**, 1563 (1993).
[53] L. Lapikás, Nucl. Phys. **A553**, 297c (1993); D. G. Ireland, L. Lapikás, and G. Van der Steenhoven, Phys. Rev. C **50**, 1625 (1994).